Nanocrystalline Precursors for the Co-Assembly of Crack-Free Metal Oxide Inverse Opals

WILEY-VCH

DOI: 10.1002/adma.201706329
Article type: Communication

Nanocrystalline Precursors for the Co-Assembly of Crack-Free Metal Oxide Inverse Opals

*Katherine R. Phillips, Tanya Shirman, Elijah Shirman, Anna V. Shneidman, Theresa M. Kay, and Joanna Aizenberg**

Dr. K. R. Phillips and Prof. J. Aizenberg
Department of Chemistry and Chemical Biology, Harvard University, Cambridge, MA 02138, USA
Email: jaiz@seas.harvard.edu

Dr. T. Shirman, Dr. E. Shirman, Dr. A. V. Shneidman, T. Kay, and Prof. J. Aizenberg
John A. Paulson School of Engineering and Applied Sciences, Harvard University, Cambridge, MA 02138, USA

Dr. T. Shirman, Dr. E. Shirman, and Prof. J. Aizenberg
Wyss Institute for Biologically Inspired Engineering, Harvard University, Cambridge, MA 02138, USA

Keywords: inverse opals, titania nanocrystals, self-assembly

Inorganic microstructured materials are ubiquitous in nature. However, their formation in artificial self-assembly systems involves a complex interplay of competing forces during and after assembly. For example, colloidal assembly requires fine-tuning of factors such as the size and surface charge of the particles and electrolyte strength of the solvent to enable successful self-assembly and minimize crack formation. Co-assembly of templating colloidal particles together with a sol-gel matrix precursor material helps to release stresses that accumulate during drying and solidification, as previously shown for the formation of high quality inverse opal (IO) films out of amorphous silica. Expanding

this methodology to crystalline materials would result in microscale architectures with enhanced photonic, electronic, and catalytic properties. This work describes tailoring the crystallinity of metal oxide precursors that enable the formation of highly ordered, large area (millimeters^2) crack-free titania, zirconia, and alumina IO films. The same bio-inspired approach can be applied to other crystalline materials as well as structures beyond IOs.

Nature creates complex microstructures with advanced functionality by controlling the chemistry and morphology of the nanoscale building blocks. In order to achieve high-quality microscale architectures using synthetic self-assembly, the material precursors must also be carefully tailored. One of the most popular natural and synthetic self-assembled materials, opals, are periodic porous structures created through assembly of monodisperse spherical sub-micron colloidal particles, which are often used as a template to form inverse opals (IOs). These structures exhibit unique optical, mechanical, and fluidic properties,[1] but a high degree of control over their composition and quality is important for many of their applications, including non-fading pigments,[2] color displays,[3] solar cells,[4] catalysts,[1e, 5] and filtration membranes.[6] Structural defects, such as cracks, can be detrimental to IO's performance in these applications, as they lead to optical scattering and fluid escape paths. In order to avoid such defects, nature often utilizes soft, typically organic, entities to direct the deposition of inorganic materials.[7] Inspired by this strategy, our group previously introduced a co-assembly method, in which templating colloidal particles and matrix precursor materials are deposited

simultaneously from a single assembly mixture to produce defect-free IO films over centimeter scales.[8] Co-assembly mitigates crack formation during the drying process due to the presence of mobile colloidal particles (**Figure S1**), contrasting with the rigid template for the typical alternative approach, which involves backfilling a pre-formed colloidal template, and which results in high-quality domains of no more than 10-100 μm in each direction.[9]

Co-assembly has enabled crack-free IOs out of amorphous materials such as silica. By extending the co-assembly process to crystalline metal oxides, such as titania and alumina, the benefits of long-range order can be combined with inherent materials properties, i.e. high refractive index and reactivity. Additionally, fundamental questions related to photonic-enhanced photocatalysis[10] and band-edge lasing[11] could be investigated with IO films. However, the formation of defect-free metal oxide IOs remains a challenge in part due to the amorphous-to-crystalline phase transition and associated crystallization-induced volume shrinkage of solid matrix during the heat treatment, whether purely crystalline precursors,[12] amorphous sol-gel precursors,[13] or a combination of both[14] are used. Metal oxide sol-gel precursors present the additional challenge of high hydrolytic instability.[15]

Nature again provides inspiration as we look to expand the scope of inverse opal composition to include crystalline materials. One of the central biomineralization principles is to pre-assemble nanoscale building blocks with controlled surface charge,

size, shape, and crystallinity.[7] In particular, the formation of crystalline and amorphous phases that coexist in mineralized tissues, as well as amorphous-to-crystalline transitions, are common, very general biomineralization principles that endow crystalline biomaterials with high order and mechanical stability.[16] By combining amorphous ("soft") and crystalline ("hard") components with optimized ratio and dimensions of the building blocks, nature forms structures with fine features that experience minimal structural changes during densification and phase transitions.[17]

This work describes a generalized approach for the co-assembly of crack-free metal oxide (titania, zirconia, and alumina) IO films based on precursors designed with the same biomineralization principle (**Figure 1**). We report that a careful choice of nanocrystalline metal oxide precursors (NCs) containing finely controlled proportions of crystalline and amorphous phases allows us to achieve this goal. As discussed in SI and shown in **Figures S1-3**, the amorphous portion of the NCs mitigates stresses arising during the colloidal assembly process, and the crystalline component minimizes large volume shrinkage arising during calcination-induced phase transitions. Furthermore, we demonstrate the applicability of this method to grow inverse opal films on flexible substrates as well as to incorporate additional functional nanoparticles.

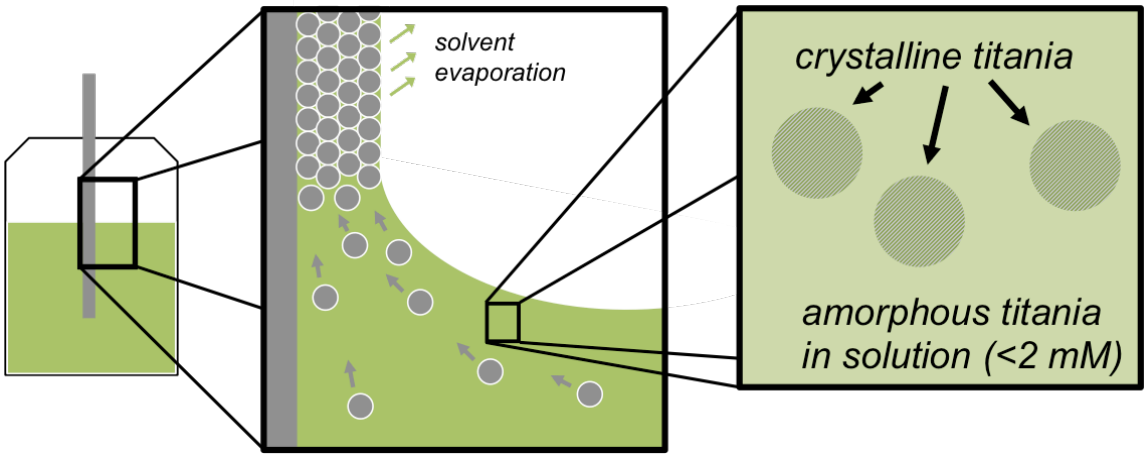

Figure 1. Schematic of co-assembly process via evaporation-induced deposition of templating colloids and titania precursor on a vertical substrate. The titania nanocrystalline precursor consists of titania in various crystalline and amorphous phases.

A published peptization process[18] provided control over titania NC size, morphology and their amorphous fraction. The synthesis procedure is based on hydrolysis and poly-condensation of titanium alkoxide in the presence of tetramethylammonium hydroxide (TMAH).[18] It has been suggested that TMAH catalyzes a complete hydrolysis of alkoxide groups and provides an organic cation to assist and direct the polycondensation process (nucleation and growth), by stabilizing the intermediate structural units or clusters (see SI for more details).[18] Here, a constant amount (41.3 mM) of titanium isopropoxide (TIP) in 2-propanol was added dropwise to a precooled aqueous solution of TMAH; the concentration of TMAH was varied to achieve molar ratios of TIP to TMAH ($R_{TIP/TMAH}$) between 0.3 and 2.0. The reaction mixture was then refluxed and cooled, and allowed to age for specific times. The resulting suspended precursors were dried and subsequently characterized by transmission electron microscopy (TEM), Raman spectroscopy, X-ray diffraction (XRD), X-ray photoelectron spectroscopy (XPS), thermal

gravimetric analysis (TGA), and differential scanning calorimetry (DSC), and both the concentration of TMAH and the aging of the particles were shown to affect the NC size and morphology.

TEM and Raman spectra indicate that titania is present in the anatase phase. TEM micrographs show crystalline particles for all $R_{TIP/TMAH}$>0.3; however, the degree of crystallinity and their size depends on TIP/TMAH molar ratio and aging (**Figure S4**). As shown in **Figure 2A-C,** the lattice planes have an interplanar distance of 3.5 Å for $R_{TIP/TMAH}$=1 and 1.4, corresponding to the (101) planes of the anatase crystal structure.[19] Raman spectroscopy further confirms the presence of the anatase phase (**Figure 2D)**, with the primary characteristic anatase Eg Raman modes visible at ~146 cm^{-1} for $R_{TIP/TMAH}$>1.4. NCs with $R_{TIP/TMAH}$=0.5 and 1.0 show no anatase Raman peaks despite the TEM results, which we attribute to the presence of large amount of amorphous titania. In terms of morphology, NCs with R≤1.4 ratio are ~5 nm with nearly spherical shape. For higher TIP/TMAH ratios, the NC size increases to ~20-30 nm for $R_{TIP/TMAH}$=2 and they form elongated fibers (**Figure S5**). The increase of the crystallite size is further confirmed by the shift in the main Eg Raman band frequency, as shown in the inset of **Figure 2D**, in accordance with the phonon confinement model.[20] Aging time also influences the crystallinity and morphology of the titania NCs, as discussed in more detail in the SI.

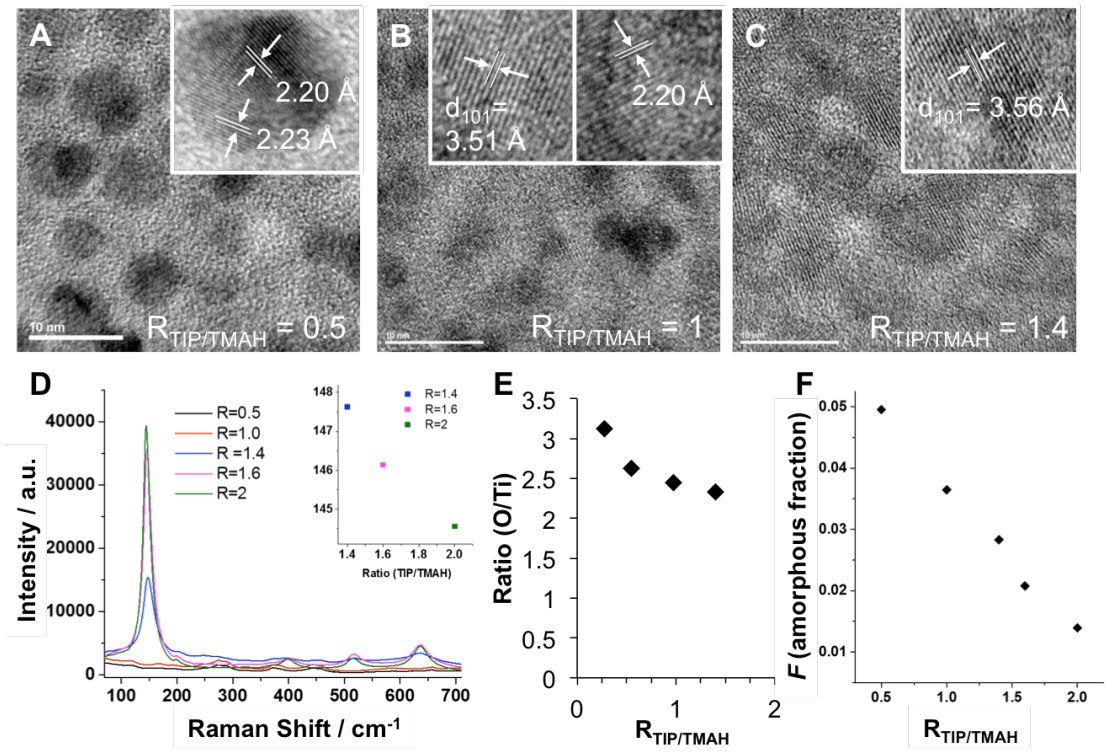

Figure 2. Imaging and characterization of as-synthesized titania nanocrystalline precursors made with different ratios ($R_{TIP/TMAH}$) of titanium precursor (titanium isopropoxide, TIP) to base (tetramethylammonium hydroxide, TMAH). (A-C) TEM images of nanocrystals with $R_{TIP/TMAH}$ of (A) 0.5, (B) 1, and (C) 1.4, all after 7 days aging. (D-E) Analytical spectroscopy: (D) Raman spectra of titania nanocrystalline precursors prepared using various $R_{TIP/TMAH}$ before calcination, with aging time of 7 days; inset shows red-shift (to lower cm^{-1}) of the characteristic anatase titania peak frequencies with increasing $R_{TIP/TMAH}$. (E) Ratio of O to Ti, as determined by X-ray photoelectron spectroscopy (XPS) for different $R_{TIP/TMAH}$. (F) The amorphous fraction, *F*, obtained from thermal gravimetric analysis.

In order to gain insight into the relative amounts of amorphous and crystalline components of the titania NCs, we performed XPS, TGA, and DSC to probe the degree of condensation of $Ti(OH)_x$ species in different NCs. XPS measurements were performed on dried NCs of different TIP/TMAH ratios after 1 month aging time. All studied samples exhibited O:Ti ratio between ~2.2 and ~3.5 (well over the stoichiometric value of 2.0 for TiO_2), which decreased noticeably for higher TIP/TMAH ratios (**Figure 2E**). Dried samples were also analyzed with TGA and DSC up to 1400 ˚C (**Figure S6**). The

weight loss around 500 ˚C in the TGA spectra corresponds to polycondensation and crystallization of hydrated titania into anatase, which can be assigned to the first broad exothermic peak on the DSC curve. Comparing the TGA/DSC data, a clear trend can be observed: the final weight loss decreases for higher TIP/TMAH ratios (lower TMAH concentrations). A quantitative comparison of t~~T~~he amorphous fraction, *F*, for samples aged for 1 month, was estimated according to Equation 1 and plotted in **Figure 2F**.

$$F = \frac{(weight\ at\ 200\ ℃) - (weight\ at\ 1000℃)}{(weight\ at\ 1000℃)} \quad (1)$$

These results support our hypothesis that higher TIP/TMAH ratios have more titania in the form of anatase crystallites. In addition to TGA and DSC, temperature effects were probed by analyzing the NCs ~~were analyzed~~ after calcination at 500 ˚C with Raman and XRD (**Figure S7**). The spectral peaks indicate that only the anatase phase of titania is formed in this temperature range. The second exothermic peak on the DSC curve, at ~1200 ˚C, was attributed to the phase transformation from anatase to rutile (see SI for more discussion).

The quality of the titania IOs co-assembled using the as-prepared NC suspension is a function of the NC properties. Depending on the titania NCs' $R_{TIP/TMAH}$ and aging, crack-free titania IO films can form (**Figure 3**). For the lowest TIP/TMAH ratios investigated, both the excess of TMAH and lack of crystalline phase result in the crack formation ($R_{TIP/TMAH}$ = 0.3, **Figure S8**). High concentrations of charged molecules such as TMAH can interfere with inter-colloidal particle repulsive forces, causing disordered films or

aggregated solutions, such as those seen for $R_{TIP/TMAH}$ = 0.3. For NCs with $R_{TIP/TMAH}$ = 0.5 and above, the lower amount of TMAH produces ordered and crack-free IO films before calcination (**Figure S9**); however, the short (1 day) NC aging times with the TIP/TMAH ratio of 0.5 yielded cracked IO films, which we attribute to an insufficient amount of crystalline titania. Aging for 7 days significantly improves the quality of the film, leading to crack-free IO films (**Figure 3A**).

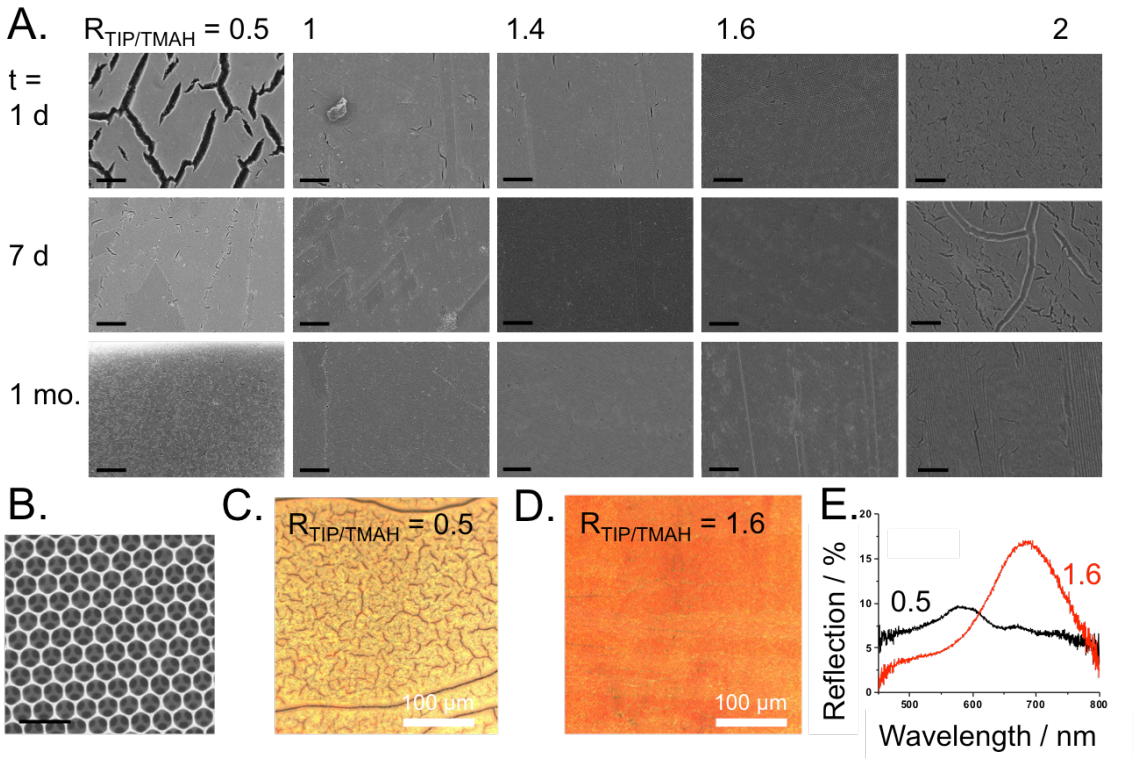

Figure 3. Inverse opal films made from various titania nanocrystals. (A) SEM images of titania inverse opal films, where each column corresponds to a different $R_{TIP/TMAH}$ ratio (from left to right): 0.5, 1, 1.4, 1.6, and 2. Each row represents a different aging time (1 day, 7 days, and 1 month). Scale bars are 10 µm. (B) SEM image of titania inverse opal film synthesized using NC's with $R_{TIP/TMAH}$ = 0.5 and 7 days aging. Scale bar is 1 µm. (C-D) Optical images, and (E) corresponding optical spectra, of titania inverse opal films made from NCs synthesized with ratios ($R_{TIP/TMAH}$) of (C) 0.5, and (D) 1.6, and 1 day aging time; scale bars are 100 µm. All samples underwent calcination at 500°C.

Higher ratios ($R_{TIP/TMAH}$ = 1, 1.4, 1.6) give rise to the formation of crack-free IO films for aging times above 1 month. The low concentration of TMAH does not disrupt the assembly, the presence of amorphous titania helps to accommodate stress during drying, and a sufficient amount of crystalline phase prevents volume shrinkage during the calcination. For NC synthesized from high TIP/TMAH ratios (such as $R_{TIP/TMAH}$=2), an increase in crack formation of the resulting IO films was observed for longer aging times. Only a freshly prepared precursor gives rise to the crack-free IO, whereas aging times longer than 1 day produce films exhibiting cracks for these precursors. The cracks are formed during the co-assembly process (**Figure S9D**), which we attribute to the large size of the titania NC precursors. From this analysis, we conclude that an amorphous fraction, *F*, between 0.02 and 0.05 is necessary to co-assemble crack-free titania IO films. All films exhibit high order (**Figure 3B**). To examine the effect of high temperature on the structural integrity, titania inverse opal films (synthesized from NC's with $R_{TIP/TMAH}$ = 1, 14 days aging) were calcined at 700 °C. The resulting films retain their spherical pore structure and showed no cracking (**Figure S10**).

Optical characterization of IOs fabricated using different NCs reveals the formation of either visible cracks (**Figure 3C**) or high quality crack-free films (**Figure 3D**) for representative precursors made with $R_{TIP/TMAH}$ of 0.5 and 1.6, respectively, both with 1 month aging time. The quality of the film also affects the reflection spectra (**Figure 3E**). The cracks in the sample made from the lower $R_{TIP/TMAH}$ show low intensity reflection peaks compared to samples made from higher $R_{TIP/TMAH}$, in addition to less vibrant colors

visible in the optical images, as expected based on the cracking seen in SEM. For titania NCs made with $R_{TIP/TMAH}$ = 1.8, a characteristic refractive index of the anatase phase of 2.23 was measured using ellipsometry (**Figure S11**). As expected, titania IOs retain color in liquids upon infiltration (**Figure S12**) due to the high refractive index of titania, which does not match that of the liquid.

This process of fabricating crack-free metal oxide inverse opal films can be applied to manufacturing various functional materials with highly desired properties and promising applications. For example, formation of IOs using metal oxides such as titania and alumina is particularly relevant for catalysis and electrode applications.[1c, 1e, 5b] Using co-assembly, we can also incorporate functional nanoparticles into the IO matrix.[2b, 21] By simply adding negatively charged (citrate-capped) gold nanoparticles (AuNP) to the NC titania precursor, we fabricated highly ordered hybrid inverse opal films with homogeneously distributed AuNP (**Figure S13**). Hybrid metal oxide support/metal nanoparticle systems are used extensively in catalysis,[5b] and titania-AuNP IOs are particularly promising photocatalytic systems.[9a]

Furthermore, titania IO films also have promising applications in the field of electrochromic (EC) devices, due to significantly faster switching times and enhanced coloration contrasts.[22] They are conventionally made by atomic layer deposition (ALD) on transparent substrates, for example indium tin oxide (ITO)-coated glass. However, the substrate choice is limited by the high temperatures that are typically required to

crystallize the matrix material and remove the templating colloids, preventing the use of inexpensive, lightweight, and flexible substrates.[23] The crystalline character of these NC precursors allows us to avoid the calcination step, instead removing the colloids by dissolution in organic solvent such as toluene. Here, we fabricated large-area crack-free titania inverse opal films on ITO-coated flexible polyethyleneterephthalate (ITO/PET) substrates (**Figure 4C,D**) that would otherwise degrade at high temperatures. As shown in the left inset of **Figure 4D**, titania inverse opal films on ITO/PET substrates retain their integrity while bent, and SEM imaging confirms that the inverse opal structure remains intact after bending (**Figure 4D**).

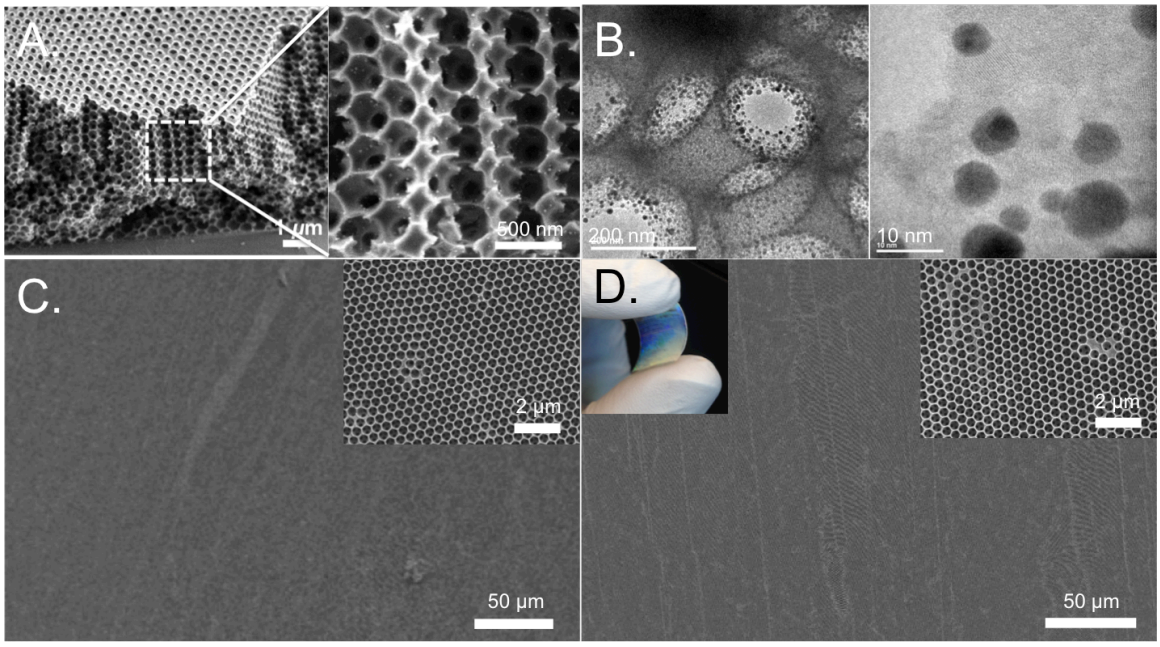

Figure 4. (A) SEM, and (B) TEM of a titania IO film with incorporated gold nanoparticles. (C-D) SEM images of a large-area, crack-free titania IO film on a conductive plastic substrate (ITO/PET), (C) before bending, and (D) after bending. Right insets show higher magnification SEM images. Left inset in (D) is a photograph of the bending.

The TMAH-based peptization process described here can be directly extended to metal oxides beyond titania, as we show for zirconia and alumina. Zirconium isopropoxide and aluminum isopropoxide were substituted for titanium isopropoxide in the NC synthesis procedure to make zirconia and alumina NCs, respectively (**Figure 5**). TEM images reveal that the resulting nanoparticles are crystalline and several nanometers in diameter (**Figure 5A,C**, insets). The SEM images show the crack-free quality of the thus-assembled IO films (**Figure 5**). The composition of the inverse opal films was confirmed using EDS and XRD (**Figure S13 and S14**).

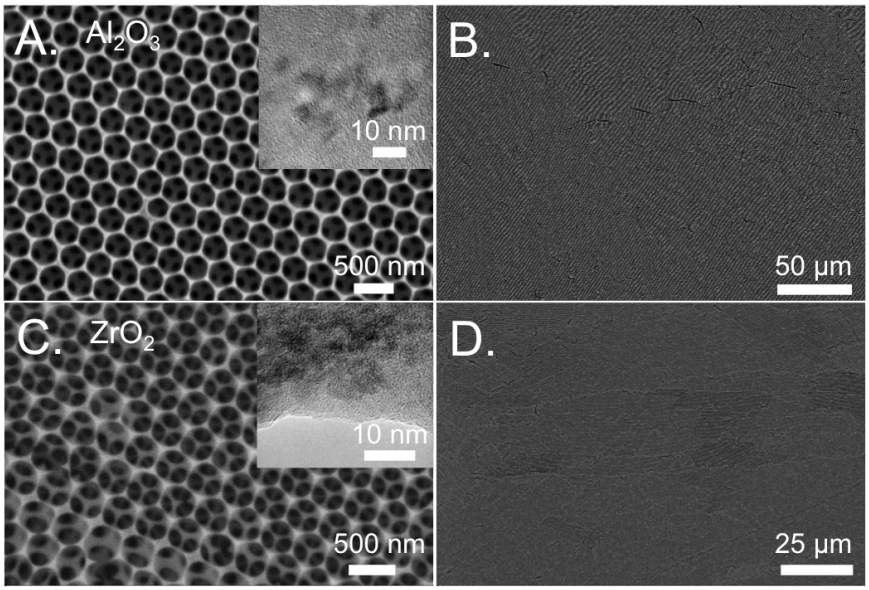

Figure 5. Representative images of inverse opal films made from (A-B) alumina, and (C-D) zirconia, grown on silicon substrates using (A, inset) Al_2O_3 nanocrystals and (C, inset) ZrO_2 nanocrystals, respectively.

In summary, crack-free titania, alumina, and zirconia IOs were co-assembled using carefully designed NC precursors. Building on biomineralization principles, where

crystalline materials often form through the amorphous-to-crystalline transitions, and where the combination of nanocrystalline and amorphous mineral phases give rise to oriented, high-quality crystals,[16] our precursors contain a mixture of nanocrystalline and amorphous metal oxide phases. Having both components allows the precursor to accommodate stresses during the self-assembly process and to minimize volume changes during phase transitions, leading to high-quality inverse opal films: the crystalline phase suppresses crack formation during calcination, and the hydrated amorphous phase suppresses crack formation during the drying stage. It is noteworthy that neither the assembly of purely crystalline precursor phase[12] nor the use of sol-gel amorphous precursors[13] nor a simple combination of both[14] allows for the formation of such ordered, defect-free crystalline metal oxide films. These crack-free IOs enable or enhance a range of applications and model studies in which the effect of the structure can be isolated without interference from defects, such as photocatalysis[10] and band-edge lasing[11] studies. In addition to crack-free titania IO films, we extended the fabrication procedure to IO films with other metal oxides (zirconia and alumina) as the matrix, as well as demonstrated their use on flexible substrates and with additional functional particles (gold nanoparticles). The presented methodology for the formation of NC precursors can be applied to other crystalline materials, and to the fabrication of a variety of nanoscale structures.

Experimental Section

Nanocrystal synthesis: Titania NCs were synthesized by modifying a peptization synthesis procedure from the literature.[18] For each batch, 25% tetramethyl ammonium

hydroxide (TMAH; up to 4.6 mL) was added to water (90 mL) in an ice bath. The exact volume of TMAH was adjusted as described in the text to achieve a desired molar ratio of titanium isopropoxide (TIP) to TMAH ($R_{TIP/TMAH}$). TIP (1.1 mL) in isopropanol (15 mL) was added dropwise to the cooled TMAH solution under stirring. After ~10 min, the flask containing the synthesis reaction was submerged in a silicone oil bath heated above 100°C, and the solution was left under reflux with a condenser for 6 h. During this time, a white gel-like precipitate formed, which slowly dissolved upon reflux. After reflux, the NCs were cooled to room temperature and the resulting suspension was used without further purification, either immediately or after aging for various lengths of time. The same procedure was followed for alumina and zirconia ~~other metal oxides~~ precursors by substituting aluminum ~~the corresponding~~ isopropoxide~~s~~ and zirconium isopropoxide, respectively, for TIP using ~~in~~ the same molar ratios.

Inverse opal assembly: IOs were made by modifying the evaporation-induced co-assembly procedure described elsewhere.[8] Briefly, acrylic-acid-capped polystyrene (PS) spheres were made following a literature procedure,[24] used after dialysis cleaning. They were diluted to 0.1% sc for assembly, to which we added the as-synthesized titania, alumina, or zirconia NCs (40 µL~~) or other NCs (described above)~~ per mL of assembly solution). When used, citrate-capped AuNP (100 µL) were added per mL of assembly solution.

A silicon wafer or glass slide was used as substrate, which underwent plasma cleaning prior to use. For the samples grown on ITO/PET, the ITO-coated plastic

substrates were first cleaned for 3 min in an ultrasonic bath in acetone, ethanol, and deionized water, successively, then dried, and finally plasma-treated for 1 min. The substrate was suspended vertically in the center of the vial, with the end of the substrate submerged into the assembly solution but not touching the bottom of the vial. The vial was then placed in a 65°C oven and left undisturbed for several days for the co-assembly process to occur. Typically, the samples next underwent calcination at 500 ˚C for 2 h to sinter the matrix and remove the PS template. For samples grown on ITO/PET, the PS colloids were removed by dissolution in toluene.

Supporting Information

Supporting Information is available from the Wiley Online Library or from the author.

Acknowledgements

K. R. P and T. S. contributed equally to this work. The authors acknowledge Dr. Alison Grinthal and Dr. Michael Aizenberg for thoughtful discussions and assistance with the manuscript. K.R.P. acknowledges support from a graduate fellowship from the Department of Defense. T.S. acknowledges support from the Weizmann Institute of Science—National Postdoctoral Award Program for Advancing Women in Science. Electron microscopy and other characterizations were performed at the Center for Nanoscale Systems (CNS) at Harvard University, supported by the NSF under award number ECS-0335765.

References

[1] a) J. F. Galisteo-Lopez, M. Ibisate, R. Sapienza, L. S. Froufe-Perez, A. Blanco, C. Lopez, *Adv Mater* **2011**, *23*, 30-69; b) N. D. Petkovich, A. Stein, *Chem. Soc. Rev.* **2013**, *42*, 3721-3739; c) K. R. Phillips, G. T. England, S. Sunny, E. Shirman, T. Shirman, N. Vogel, J. Aizenberg, *Chem. Soc. Rev.* **2016**, *45*, 281-322; d) A. Stein, F. Li, N. R. Denny, *Chem. Mater.* **2008**, *20*, 649-666; e) A. Stein, B. E. Wilson, S. G. Rudisill, *Chem. Soc. Rev.* **2013**, *42*, 2763-2803; f) G. von Freymann, V. Kitaev, B. V. Lotsch, G. A. Ozin, *Chem. Soc. Rev.* **2013**, *42*, 2528-2554.

[2] a) D. P. Josephson, M. Miller, A. Stein, *Z. Anorg. Allg. Chem.* **2014**, *640*, 655-662; b) N. Koay, I. B. Burgess, T. M. Kay, B. A. Nerger, M. Miles-Rossouw, T. Shirman, T. L. Vu, G. England, K. R. Phillips, S. Utech, N. Vogel, M. Kolle, J. Aizenberg, *Opt. Express* **2014**, *22*, 27750-27768.

[3] a) T. Ito, C. Katsura, H. Sugimoto, E. Nakanishi, K. Inomata, *Langmuir* **2013**, *29*, 13951-13957; b) S. Y. Lee, S. H. Kim, H. Hwang, J. Y. Sim, S. M. Yang, *Adv. Mater.* **2014**, *26*, 2391-2397.

[4] a) X. Chen, J. Ye, S. Ouyang, T. Kako, Z. Li, Z. Zou, *ACS Nano* **2011**, *5*, 4310-4318; b) S. Guldin, S. Huttner, M. Kolle, M. E. Welland, P. Muller-Buschbaum, R. H. Friend, U. Steiner, N. Tetreault, *Nano Lett.* **2010**, *10*, 2303-2309; c) J. W. Lee, J. Lee, C. Kim, C. Y. Cho, J. H. Moon, *Sci. Rep.* **2014**, *4*, 6804; d) J. W. Lee, J. H. Moon, *Nanoscale* **2015**, *7*, 5164-5168.

[5] a) C. M. Parlett, M. A. Isaacs, S. K. Beaumont, L. M. Bingham, N. S. Hondow, K. Wilson, A. F. Lee, *Nat. Mater.* **2016**, *15*, 178-182; b) E. Shirman, T. Shirman, A. V. Shneidman, A. Grinthal, K. R. Phillips, H. Whelan, E. Bulger, M. Abramovitch, J. Patil, R. Nevarez, J. Aizenberg, *Adv. Funct. Mater.* **2017**, DOI: 10.1002/adfm.201704559; c) Y. Wang, H. Arandiyan, J. Scott, M. Akia, H. Dai, J. Deng, K.-F. Aguey-Zinsou, R. Amal, *ACS Catalysis* **2016**, *6*, 6935-6947.

[6] a) D. Li, J. Yao, H. Wang, in *Encyclopedia of Membrane Science and Technology*, **2013**; b) X. Wang, S. M. Husson, X. Qian, S. R. Wickramasinghe, *J. Membrane Sci.* **2010**, *365*, 302-310; c) S. J. Yeo, G. H. Choi, P. J. Yoo, *J. Mater. Chem. A* **2017**, *5*, 17111-17134.

[7] a) L. Addadi, S. Weiner, *Angew Chem Int Ed Engl* **1992**, *31*, 153-169; b) P. U. P. A. Gilbert, M. Abrecht, B. H. Frazer, *Rev. Mineral. Geochem.* **2005**, *59*, 157-185; c) C. Rodriguez-Navarro, E. Ruiz-Agudo, J. Harris, S. E. Wolf, *J. Struct. Biol.* **2016**, *196*, 260-287; d) S. Weiner, L. Addadi, *Ann. Rev. Mater. Res.* **2011**, *41*, 21-40.

[8] B. Hatton, L. Mishchenko, S. Davis, K. H. Sandhage, J. Aizenberg, *Proc Natl Acad Sci U S A* **2010**, *107*, 10354-10359.

[9] a) Z. Cai, Z. Xiong, X. Lu, J. Teng, *J. Mater. Chem. A* **2014**, *2*, 545-553; b) J. I. L. Chen, G. von Freymann, S. Y. Choi, V. Kitaev, G. A. Ozin, *Adv. Mater.* **2006**, *18*, 1915-1919; c) K. Kim, P. Thiyagarajan, H. J. Ahn, S. I. Kim, J. H. Jang, *Nanoscale* **2013**, *5*, 6254-6260; d) J. Liu, M. Li, J. Wang, Y. Song, L. Jiang, T. Murakami, A. Fujishima, *Environ. Sci. & Technol.* **2009**, *43*, 9425-9431.

[10] M. Curti, J. Schneider, D. W. Bahnemann, C. B. Mendive, *J. Phys. Chem. Lett.* **2015**, *6*, 3903-3910.

[11] a) J. P. Dowling, M. Scalora, M. J. Bloemer, C. M. Bowden, *J. Appl. Phys.* **1994**, *75*, 1896-1899; b) M. Scharrer, H. Noh, X. Wu, M. A. Anderson, A. Yamilov, H. Cao, R. P. H. Chang, *J. Optics* **2010**, *12*, 024007; c) O. Toader, S. John, K. Busch, *Opt. Express* **2001**, *8*, 217; d) C.-F. Ying, W.-Y. Zhou, Q. Ye, X.-L. Zhang, J.-G. Tian, *J. Optics* **2010**, *12*, 115101.

[12] a) C. Y. Cho, J. H. Moon, *Langmuir* **2012**, *28*, 9372-9377; b) Y. G. Seo, M. A. Kim, H. Lee, W. Lee, *Sol. Energy Mater. Sol. Cells* **2011**, *95*, 332-335; c) J. H. Shin, J. H. Kang, W. M. Jin, J. H. Park, Y. S. Cho, J. H. Moon, *Langmuir* **2011**, *27*, 856-860.

[13] a) C. Dionigi, G. Calestani, T. Ferraroni, G. Ruani, L. F. Liotta, A. Migliori, P. Nozar, D. Palles, *J. Colloid Interface Sci.* **2005**, *290*, 201-207; b) J. W. Galusha, C.-K. Tsung, G. D. Stucky, M. H. Bartl, *Chem. Mater.* **2008**, *20*, 4925-4930; c) F. Jia, W. Sun, J. Zhang, Y. Li, B. Yang, *J. Mater. Chem.* **2012**, *22*, 2435-2441.

[14] a) B. Mandlmeier, N. K. Minar, J. M. Feckl, D. Fattakhova-Rohlfing, T. Bein, *J. Mater. Chem. A* **2014**, *2*, 6504-6511; b) J. M. Szeifert, D. Fattakhova-Rohlfing, D. Georgiadou, V. Kalousek, J. Rathouský, D. Kuang, S. Wenger, S. M. Zakeeruddin, M. Grätzel, T. Bein, *Chem. Mater.* **2009**, *21*, 1260-1265.

[15] V. G. Kessler, *J. Sol-Gel Sci. Technol.* **2013**, *68*, 464-470.

[16] a) J. J. De Yoreo, *MRS Bulletin* **2017**, *42*, 525-536; b) L. B. Gower, *Chem. Rev.* **2008**, *108*, 4551-4627; c) X. Ma, S. Zhang, F. Jiao, C. J. Newcomb, Y. Zhang, A. Prakash, Z. Liao, M. D. Baer, C. J. Mundy, J. Pfaendtner, A. Noy, C. L. Chen, J. J. De Yoreo, *Nat. Mater.* **2017**, *16*, 767-774; d) C. C. Perry, S. V. Patwardhan, O. Deschaume, *Biochem. Soc. Trans.* **2009**, *37*, 687-691.

[17] V. Thota, C. C. Perry, *Recent Pat. Nanotechnol.* **2017**, *11*, 168-180.

[18] A. Chemseddine, T. Moritz, *Eur. J. Inorg. Chem.* **1999**, *1999*, 235-245.

[19] L. Miao, P. Jin, K. Kaneko, A. Terai, N. Nabatova-Gabain, S. Tanemura, *Appl. Surf. Sci.* **2003**, *212-213*, 255-263.

[20] X. Xue, W. Ji, Z. Mao, H. Mao, Y. Wang, X. Wang, W. Ruan, B. Zhao, J. R. Lombardi, *J. Phys. Chem. C* **2012**, *116*, 8792-8797.

[21] Y. Vasquez, M. Kolle, L. Mishchenko, B. D. Hatton, J. Aizenberg, *ACS Photonics* **2014**, *1*, 53-60.

[22] C. G. Granqvist, *Sol. Energy Mater. Sol. Cells* **2012**, *99*, 1-13.

[23] H. Li, G. Vienneau, M. Jones, B. Subramanian, J. Robichaud, Y. Djaoued, *J. Mater. Chem. C* **2014**, *2*, 7804.

[24] J. Goodwin, J. Hearn, C. Ho, R. H. Ottewill, *Colloid Polym. Sci.* **1974**, *252*, 464-471.